Nonrigid Registration Using a Rigidity Constraint

Marius Staring, Stefan Klein and Josien P.W. Pluim

Image Sciences Institute, University Medical Center Utrecht,
P.O. Box 85500, 3508 GA, Room Q0S.459, Utrecht, The Netherlands

ABSTRACT

Nonrigid registration is a technique commonly used in the field of medical imaging. A drawback of most current nonrigid registration algorithms is that they model all tissue as being nonrigid. When a nonrigid registration is performed, the rigid objects in the image, such as bony structures or surgical instruments, may also transform nonrigidly. Other consequences are that tumour growth between follow-up images may be concealed, or that structures containing contrast material in one image and not in the other may be compressed by the registration algorithm.

In this paper we propose a novel regularisation term, which is added to the cost function in order to penalise nonrigid deformations of rigid objects. This regularisation term can be used for any representation of the deformation field capable of modelling locally rigid deformations. By using a B-spline representation of the deformation field, a fast algorithm can be devised. We show on 2D synthetic data, on clinical CT slices, and on clinical DSA images, that the proposed rigidity constraint is successful, thus improving registration results.

Keywords: nonrigid registration, rigidity constraint, regularisation, rigid penalty term

1. INTRODUCTION

Popular image registration algorithms, like described by Rueckert *et al.*[1] and Mattes *et al.*,[2] usually do not take the rigidity of different tissue types into account. If rigid objects like bones or surgical instruments are present in the volume of interest, these algorithms will not necessarily preserve the rigidity of these objects.

Preservation of rigidity is not only desirable for tissue that is rigid by nature, it can also be useful in other cases. If we consider structures that change in size between two images, it could be useful to retain the difference between the two, so that from this difference the change is immediately clear. This is the case for example for follow-up images of tumours. Perfect nonrigid registration will match the two tumours, and no difference in size is observed; tumour growth is effectively concealed. Keeping the tumour rigid would prevent this. Another application where rigidity preservation is useful, is the case of pre- and post-contrast images. In, for example, digital subtraction angiography (DSA) images, vessels are present in one image and not or only partially in the other. Intensity-based registration algorithms are designed to minimise the difference between the two, resulting in the compression of the contrast-enhanced structure. This effect has been reported in literature for the case of contrast-enhanced breast lesions[3,4] and contrast-enhanced vessels in CT-DSA.[5]

Several methods to constrain deformations have been described in the literature. One that is well known and widely used is to employ a regularisation or penalty term. Typical penalty terms include the bending energy of a thin plate,[1] the linear elasticity constraint,[6,7] and the incompressibility constraint.[3] Particular methods to enforce rigidity on structures have also been proposed. Tanner *et al.*[4] propose to couple the control points of a B-spline deformation. Another approach is taken by Little *et al.*,[8] who use modified basis functions describing the deformation, constraining the nonlinear part of the deformation at rigid locations by multiplication with a weight function.

In this paper we propose a method to nonrigidly align images, while keeping rigid objects rigid. This is achieved by a novel rigidity constraint. The method is described in 2D, but can be readily extended to 3D or even nD.

Send correspondence to M. Staring
M. Staring: e-mail: marius@isi.uu.nl, telephone: +31 30 250 3186

2. METHOD

Registration of a moving image $M(\boldsymbol{x}) : \Omega_M \subset \mathbb{R}^d \mapsto \mathbb{R}$ to a fixed image $F(\boldsymbol{x}) : \Omega_F \subset \mathbb{R}^d \mapsto \mathbb{R}$, both of dimension d, consists of finding a deformation $\boldsymbol{u}(\boldsymbol{x})$ that makes $M(\boldsymbol{x} + \boldsymbol{u}(\boldsymbol{x}))$ spatially aligned to $F(\boldsymbol{x})$. The quality of alignment is defined by a similarity or distance measure $\mathcal{D}$, such as the sum of squared differences (SSD), the correlation ratio, or in our case the mutual information (MI) measure.

Because this problem is ill-posed, a regularisation term or smoother $\mathcal{S}$ is introduced and the registration problem is formulated as an optimisation problem in which the cost function $\mathcal{J}$ is minimised w.r.t. $\boldsymbol{u}$, with:

$$\mathcal{J}[F, M; \boldsymbol{u}] = \mathcal{D}[F, M; \boldsymbol{u}] + \alpha \mathcal{S}[\boldsymbol{u}], \tag{1}$$

where α weighs similarity against smoothness. Note that at the minimum the derivatives of the similarity measure and the regularisation term are not necessarily zero. Merely, a balance is found between the two, which is influenced by the parameter α.

We propose a new constraint $\mathcal{S}^{\text{rigid}}[\mathbf{u}]$ in order to keep rigid objects rigid, which we call the rigidity constraint. This penalty term can be weighted locally, so that some parts of the image are restricted to rigid movement, while other parts may be penalised partially or may deform freely.

In the following section we describe the general registration algorithm, see Section 2.1. Construction of the rigid penalty term and a proof of its validity are described in Section 2.2. Section 2.3 describes how this penalty term can be efficiently computed if the deformation field is parameterised by B-splines.

2.1. Registration algorithm

We employ a registration framework largely based on the papers of Rueckert *et al.*[1] and Mattes *et al.*[2] The similarity measure is the mutual information measure using an implementation by Thévenaz and Unser.[9] The deformation field is parameterised by cubic B-splines. A multiresolution approach is taken to avoid local minima, using a Gaussian pyramid with a subsampling factor of 2 in each dimension. Also a multiresolution approach of the deformation grid is taken: when the image resolution in the pyramid is doubled, the B-spline control point spacing is halved. For the optimisation of the cost function $\mathcal{J}$, we use a stochastic gradient descent optimiser, using only a randomly chosen portion of the total number of pixels for calculating the derivative of $\mathcal{J}$ with respect to the B-spline parameters.[10]

2.2. Construction of the rigidity constraint

In this section we derive three conditions that must hold for $\boldsymbol{u}$ to be a rigid deformation. These three conditions are combined in one penalty term, our rigidity constraint $\mathcal{S}^{\text{rigid}}[\mathbf{u}]$, constructed such that deviation from these three conditions is penalised.

For a deformation field $\boldsymbol{u}$ to be rigid, it must hold that

$$\boldsymbol{u}(\boldsymbol{x}) + \boldsymbol{x} = R\boldsymbol{x} + \boldsymbol{t}, \tag{2}$$

with R and $\boldsymbol{t}$ a rotation matrix and a translation vector, respectively. Three conditions on $\boldsymbol{u}$ can be derived:

linearity A rigid deformation is a linear function of $\boldsymbol{x}$, giving us the linearity conditions $\text{LC}_{lij}(\boldsymbol{x})$, which state that the second order derivatives of $\boldsymbol{u}$ to $\boldsymbol{x}$ are to be zero:

$$\text{LC}_{kij}(\boldsymbol{x}) = \frac{\partial^2 u_k(\boldsymbol{x})}{\partial x_i \partial x_j} = 0, \tag{3}$$

for all $k, i, j = 1, 2$, not counting duplicates.

orthonormality For the matrix R to be a rotation matrix the orthonormality conditions must hold, which state that $\sum_{k=1}^{2} r_{ki} r_{kj} = \delta_{ij}$, for all $i, j = 1, 2$, with r_{ij} the elements of R. From Equation (2) it follows that $\frac{\partial u_i}{\partial x_j} = r_{ij} - \delta_{ij}$, for all $i, j = 1, 2$. Hence, the orthonormality conditions OC_{ij} can be rewritten to

$$\mathrm{OC}_{ij}(\boldsymbol{x}) = \sum_{k=1}^{2} \left(\frac{\partial u_k(\boldsymbol{x})}{\partial x_i} + \delta_{ki} \right) \left(\frac{\partial u_k(\boldsymbol{x})}{\partial x_j} + \delta_{kj} \right) - \delta_{ij} = 0, \tag{4}$$

for all $i, j = 1, 2$, again not counting duplicates. Note that, since $r_{ij} = \frac{\partial u_i}{\partial x_j} + \delta_{ij}$, the rotation matrix R is the Jacobian of the transformation $\boldsymbol{u}(\boldsymbol{x}) + \boldsymbol{x}$.

properness A matrix R satisfying these conditions can still be proper or improper, meaning that the determinant can still be either 1 or -1, respectively. An improper orthonormal matrix corresponds to a rotation with an inversion (mirroring). Therefore we need to impose the properness condition $\mathrm{PC}(\boldsymbol{x}) = \det(R) - 1 = 0$, where the elements r_{ij} of the matrix R are again expressed in derivatives of $\boldsymbol{u}$ to $\boldsymbol{x}$. Note that, since the properness condition penalises deviations of the determinant of R from 1, and since R is the Jacobian of the transformation, this condition basically amounts to an incompressibility constraint, see also.[3]

We define the rigidity constraint $\mathcal{S}^{\mathrm{rigid}}[\boldsymbol{u}]$ to be the sum of all these conditions squared. In order to distinguish between rigid and nonrigid tissue, all the above terms are weighted by a so-called rigidity coefficient $c(\boldsymbol{x}) \in [0, 1]$ of the tissue type at position $\boldsymbol{x}$. This comes down to

$$\mathcal{S}^{\mathrm{rigid}}[\boldsymbol{u}] \triangleq \sum_{\boldsymbol{x} \in \Omega_F} c(\boldsymbol{x}) \left\{ \sum_{k,i,j} \left[\mathrm{LC}_{kij}(\boldsymbol{x}) \right]^2 + \sum_{i,j} \left[\mathrm{OC}_{ij}(\boldsymbol{x}) \right]^2 + \left[\mathrm{PC}(\boldsymbol{x}) \right]^2 \right\}. \tag{5}$$

The rigidity coefficient $c(\boldsymbol{x})$ is chosen zero for pixels $\boldsymbol{x}$ in completely nonrigid tissue, thereby not penalising deformations at those locations. For completely rigid tissue $c(\boldsymbol{x})$ is set to one. For other tissue types a value of $c(\boldsymbol{x})$ is chosen between zero and one. The rigidity coefficient image can be constructed by performing a manual or automatic segmentation of structures of interest, after which a rigidity coefficient can be assigned to it. For the case of CT images the Houndsfield units itself might be used, rescaled to the range $[0, 1]$, since more rigid tissue usually has a higher attenuation value.

The following theorem proofs the validity of the proposed rigidity constraint. For clarity, we assume that $c(\boldsymbol{x}) > 0$, for all $\boldsymbol{x} \in \Omega_F$. If this is not the case, the theorem holds for every connected subregion $\Omega_S \subset \Omega_F$ where $c(\boldsymbol{x}) > 0$, for all $\boldsymbol{x} \in \Omega_S$. For regions where $c(\boldsymbol{x}) = 0$, the deformation is unconstrained.

THEOREM 2.1. *$\mathcal{S}^{\mathrm{rigid}}[\boldsymbol{u}] = 0$ if and only if the deformation field $\boldsymbol{u}(\boldsymbol{x})$ is rigid, provided that $c(\boldsymbol{x}) > 0$, $\forall \boldsymbol{x} \in \Omega_F$.*

Proof. The *if*-part is trivial, which leaves us to prove the *only if*-part. Let $\mathcal{S}^{\mathrm{rigid}}[\boldsymbol{u}] = 0$, which is at every location $\boldsymbol{x}$ a sum of three nonnegative terms, since all terms are squared and $c(\boldsymbol{x}) > 0$, $\forall \boldsymbol{x} \in \Omega_F$. Therefore, each of the three terms is zero. Since the first term is zero, all second order derivatives are zero, making $\boldsymbol{u}(\boldsymbol{x})$ a linear function. Therefore the deformation can be written as $\boldsymbol{u}(\boldsymbol{x}) = \tilde{R}\boldsymbol{x} + \boldsymbol{t}$. Given that the second term is zero it holds that

$$\sum_{k=1}^{2} \left(\tilde{r}_{ki} + \delta_{ki} \right) \left(\tilde{r}_{kj} + \delta_{kj} \right) = \delta_{ij} \quad \forall i, j = 1, 2, \tag{6}$$

since $\frac{\partial u_i}{\partial x_j} = \tilde{r}_{ij}$. Now splitting up $\tilde{R} + I_d = R$ (giving a deformation $\mathbf{u}(\mathbf{x}) = \mathbf{R}\mathbf{x} - \mathbf{x} + \mathbf{t}$), gives $\tilde{r}_{ij} = r_{ij} - \delta_{ij}$. This rewrites Equation (6) to $\sum_{k=1}^{2} r_{ki} r_{kj} = \delta_{ij}$, $\forall i, j = 1, 2$, from which we recognise the orthonormality conditions (4) for R. A similar argument holds for the third term, resulting in the properness condition. Therefore R is a rotation matrix, and $\mathbf{u}(\mathbf{x}) + (\mathbf{x})$ represents a rigid transformation. □

Note that the proposed rigidity constraint is not dependent on the B-spline parameterisation of the deformation field. However, from a computational point of view, we can benefit from this parameterisation, as is discussed in the next section.

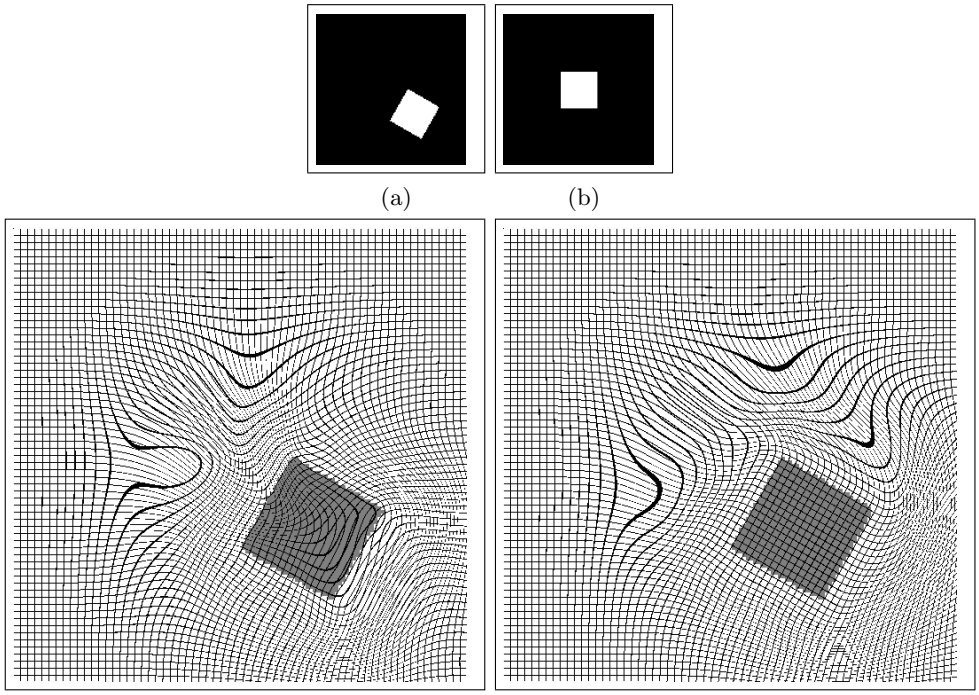

Figure 1: Comparison of registration with and without $\mathcal{S}^{\text{rigid}}[\boldsymbol{u}]$ for a 2D synthetic example. The white square is to be kept rigid. (a) fixed image, (b) moving image, (c) resulting deformation field of standard registration, and (d) resulting deformation field including the rigidity constraint.

2.3. Using B-splines

Parameterising the deformation field $\boldsymbol{u}(\boldsymbol{x})$ by B-splines, yields in 2D:

$$u_i(x_1, x_2) = \sum_{x_l \in V} \mu_{l,i} \beta^3(x_1 - x_{l,1}) \beta^3(x_2 - x_{l,2}), \tag{7}$$

for all $i = 1, 2$, with $\beta^3(x)$ the cubic B-spline polynomial, $\mu_{l,i}$ the B-spline coefficients, and V the set of all control points within the support of the B-spline. It is well-known[11] that the derivatives of $\boldsymbol{u}(\boldsymbol{x})$ can also be expressed in terms of the B-spline coefficients, using the rule

$$\frac{d\beta^n(x)}{dx} = \beta^{n-1}\left(x + \frac{1}{2}\right) - \beta^{n-1}\left(x - \frac{1}{2}\right). \tag{8}$$

Therefore also $\mathcal{S}^{\text{rigid}}[\boldsymbol{u}]$ can be expressed in terms of the B-spline coefficients $\mu_{l,i}$. We choose to evaluate the rigidity constraint only over the control points, because keeping their deformation rigid guarantees rigidity of the deformation field of points in between. This choice, combined with the compact support of B-splines, gives us an efficient way to calculate $\mathcal{S}^{\text{rigid}}[\boldsymbol{u}]$ and its derivatives (which is needed for gradient descent like optimisers).

Note that in order to define a rigid transformation at some point $\boldsymbol{x}$, all control points within the compact support of the B-spline have to be kept rigid. Therefore, one may consider dilating the rigidity coefficient image $c(\boldsymbol{x})$. However, this also results in penalising the nonrigid deformation in the neighbourhood of a rigid structure.

3. EXPERIMENTS AND RESULTS

We compare registration with the proposed rigidity constraint against registration without, in which case the cost function in Equation (1) consists only of a similarity term.

Results are first compared on 2D synthetic images in Section 3.1. To illustrate the usefulness of the rigidity constraint in situations with growth of structures, we look at selected slices of a CT follow-up thorax scan in Section 3.2. To address the problem of the compression of contrast enhanced structures, we compare registrations on 2D DSA images of the chest, see Section 3.3.

3.1. 2D synthetic examples

Rotation of a rigid object is illustrated with the square in Figure 1, where the background represents nonrigid tissue and the square a rigid object. The rigidity coefficient $c(\boldsymbol{x})$ is set to 1.0 on the square and 0.0 elsewhere. The images have dimensions of 128 by 128 pixels, and the spacing between the control points of the B-spline is chosen to be 4 pixels. For the calculation of (the derivative of) the cost function in each of the three resolutions, a subset of 1000, 4000 and 8000 pixels is used, respectively. A weight of $\alpha = 0.01$ is used.

Both algorithms give perfect registration results for the matching of the squares in Figure 1. However, the underlying deformation field is highly nonlinear if no rigid penalty term is used. If it is used the deformation field is almost perfectly rigid at the rigid part. This is also reflected in the rigidity constraint $\mathcal{S}^{\text{rigid}}[\boldsymbol{u}]$, which has a value of 2.21×10^2 for the square when computed for the result of standard nonrigid registration and a value of 1.28×10^{-3} for registration using the rigidity constraint. The rigidity constraint is not perfectly zero, because some control points outside the square, but influencing the points within the square, are not set to be rigid. Another reason is the mentioned balance between the similarity and regularisation term, see Section 2.

Figure 2 is constructed to illustrate growth. The white inner circle is translated over the image and scaled, and needs to be kept rigid during registration. Other parts of the image represent nonrigid tissue. The size of the images is 128 by 128 pixels. Registration of Figure 2b to 2a is done with a B-spline grid spacing of 8 pixels, which is necessary to be able to model the required transformation. The rigidity coefficient $c(\boldsymbol{x})$ is set to 1.0 on the inner circle representing a rigid object and 0.0 elsewhere. This rigidity coefficient image is dilated with a

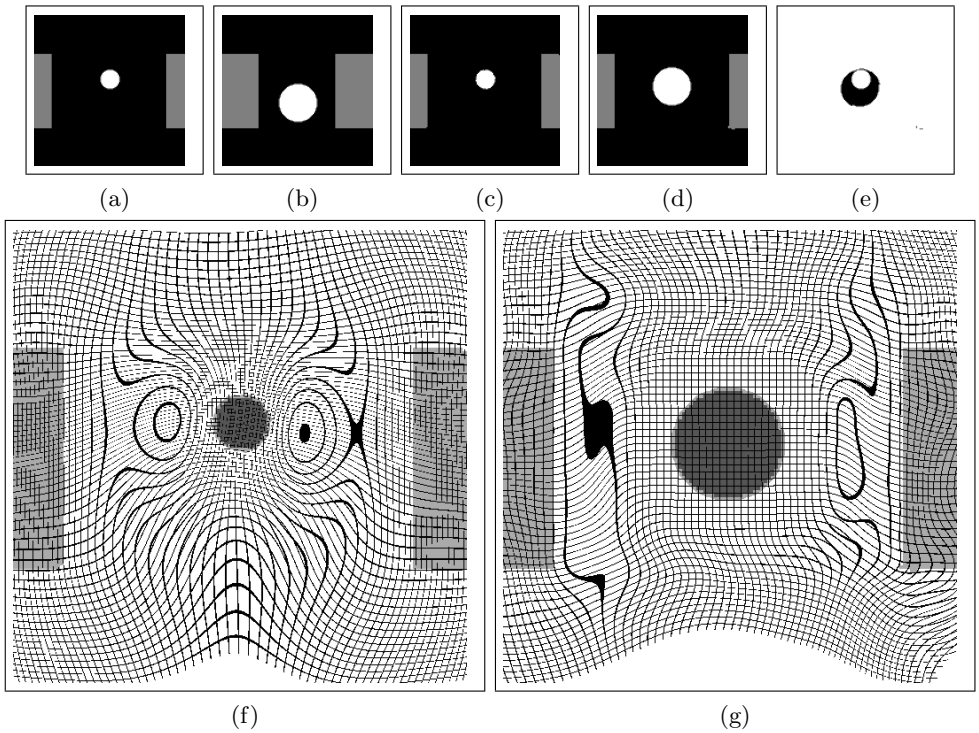

Figure 2: Comparison of registration with and without $\mathcal{S}^{\text{rigid}}[\boldsymbol{u}]$ for a 2D synthetic example. The white circle in the moving image represents a structure that is to be kept rigid. (a) fixed image, (b) moving image, (c) result of standard registration, (d) result of registration including $\mathcal{S}^{\text{rigid}}[\boldsymbol{u}]$, (e) (a) minus (d), (f) resulting deformation field of standard registration, and (g) resulting deformation field when using $\mathcal{S}^{\text{rigid}}[\boldsymbol{u}]$.

	t_0	t_1	without $\mathcal{S}^{\text{rigid}}[\boldsymbol{u}]$	with $\mathcal{S}^{\text{rigid}}[\boldsymbol{u}]$
tumour 1	736.6	1240.9	788.0	1229.0
tumour 2	136.5	180.0	137.9	185.4
tumour 3	157.7	674.2	256.6	665.4
tumour 4	0.0	170.3	92.9	179.5

Table 1: Area measurements (in mm^2) of the four tumours.

circle of radius 1.1 times the B-spline control point grid spacing. Again 1000, 4000 and 8000 samples are used for the calculation (of the derivative) of the cost function, in each resolution, respectively. The value of α is set to 0.02.

If no rigidity constraint is used the large circle in Figure 2b is compressed to the small circle in the fixed image. The area is exactly preserved for the new algorithm. The rigidity constraint has values of 3.07×10^2 and 2.00×10^{-2} without and with $\mathcal{S}^{\text{rigid}}[\boldsymbol{u}]$, respectively. As can be seen in Figure 2e the centres of the rigid circles are not aligned, because the MI-measure can not distinguish between that situation and the current one. Also note that the deformation field from Figure 2g is a rigid one at the position of the rigid object, as desired.

3.2. 2D CT follow-up slices

To be able to compare follow-up scans of a patient suffering from lung tumours by inspection of the difference image, see Figure 3a and 3d, the data sets must be registered nonrigidly. The CT data has slices of size 512 by 512 pixels, with a pixel size of 0.703125 squared for the fixed image taken at time t_0, and 0.75586 squared for the moving image taken at time t_1. In order to compare tumour volume and shape by visual inspection using the difference image, the tumours should not be deformed during registration, only rigid motion is allowed. A B-spline grid spacing of 16 voxels is used for both algorithms. In order to define rigid structures, a crude manual over-segmentation is made of the tumours, defining $c(\boldsymbol{x}) = 1.0$ in the tumour regions, and 0.0 elsewhere. 5000 pixels are used for the calculation (of the derivative) of the cost function, in all three resolutions. The value of α is set to 0.1.

As can be seen from Figure 3b, the registration algorithm without the rigid penalty term fails to keep the tumours rigid. Therefore, the difference in size due to growth can not be appreciated using the standard nonrigid registration. Using a crude segmentation of the tumours the algorithm including $\mathcal{S}^{\text{rigid}}[\boldsymbol{u}]$ succeeds in keeping the tumours rigid; from the difference image in Figure 3e it is immediately clear that the tumours have grown, whereas the rest of the image is registered nonrigidly with equal accuracy as the standard nonrigid registration. From Table 1 it can be seen that, whereas the standard registration shrinks the tumours to the size of the fixed image at t_0, adding the rigidity constraint gives volume preservation, which is a first necessity for rigidity. Several causes may explain the small deviations of the area after registration with the area at t_1. One is that not all control points influencing the tumour regions are set to enforce rigidity. This choice ensures that the deformations around the tumours are not restricted too much. Another cause is the balance between the similarity measure, which yields a force that keeps compressing the tumour, and the rigidity constraint. This balance can of coarse be influenced by the parameter α. A third cause is interpolation of the tumour segmentation, influencing the area measurements. From Figure 3f it can be appreciated that the deformation field is indeed kept rigid at the tumours, in contrast to Figure 3c.

3.3. 2D DSA images

Digital subtraction angiography (DSA) is an established modality for visualising blood vessels in the human body. During the image acquisition there is often patient motion, due to breathing, heart beat, activity in the intestines, or movement of the body. This motion results in artifacts in the subtraction images, see Figure 4c. In order to correct for this after acquisition a nonrigid registration is needed. Typically, a sequence of images is taken, where different parts of the vasculature are visible at different times. In order to see the whole imaged vasculature all those images have to be registered to the base image, which is the first image, taken just before

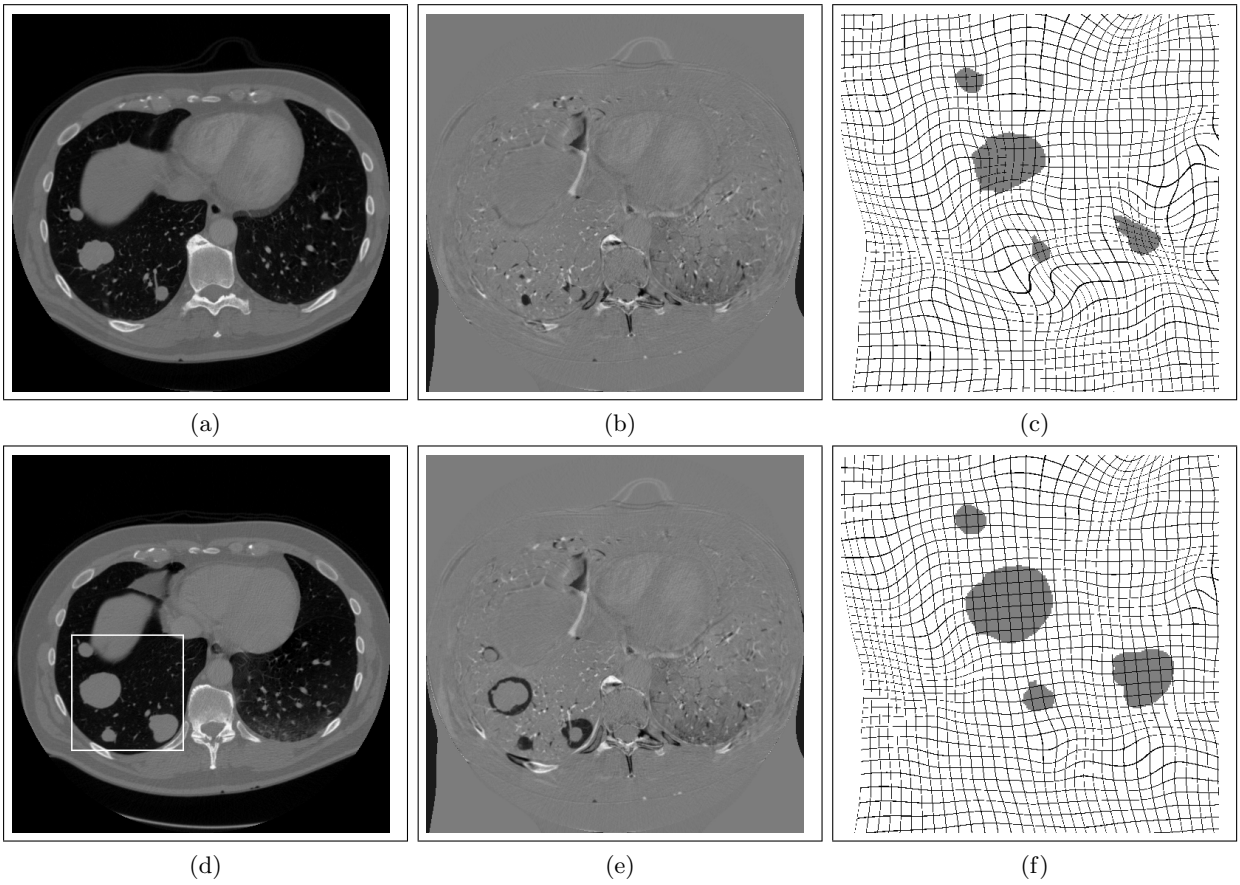

Figure 3: Comparison of registration with and without $\mathcal{S}^{\text{rigid}}[\boldsymbol{u}]$ for 2D CT thorax images. The tumours, located within the box (see (d)), have to be kept rigid for diagnostic reasons. (a) and (d): CT slice at time t_0 (the fixed image) and time t_1 (the moving image), respectively, (b) and (e): difference of the result of standard registration and rigidly regularised registration with the fixed image, respectively, (c) and (f): part of the resulting deformation field of the standard registration and of registration including $\mathcal{S}^{\text{rigid}}[\boldsymbol{u}]$, respectively.

the arrival of the contrast bolus. As reported in the literature, see Section 1, the nonrigid registration of images containing contrast enhanced structures can lead to significant compression of those structures.

We compare registration using a standard nonrigid method with the registration using the proposed rigidity constraint. The first base image is chosen to be the fixed image F, see Figure 4a, and the images containing contrast material as the moving image M, see Figure 4b. The images are of size 512 by 512 pixels, and a B-spline control point spacing of 16 pixels is used. For the case of registration with the rigidity constraint we use a crude manual over-segmentation of the vessels. 5000 pixels are used for the calculation (of the derivative) of the cost function, in all three resolutions. A value of 0.1 is assigned to α.

The registration results of the DSA images can be seen in Figure 4. Without registration and after employing a rigid registration there are still a lot of artifacts present in the background, see Figure 4c and 4d, respectively. Although nonrigid registration can compensate for this motion (Figure 4e), the vessels get severely compressed. Usage of the rigidity constraint $\mathcal{S}^{\text{rigid}}[\boldsymbol{u}]$ in the registration leaves the rigidity of the vessels intact, while removing motion artifacts in the background (Figure 4f). From the deformation fields in Figure 4g and 4h it can be seen that the standard nonrigid registration compresses the vessels, whereas the rigid penalty term preserves rigidity.

Besides visual inspection (Figure 4), the success of removal of motion artifacts in the background $\mathcal{B}$ is evaluated

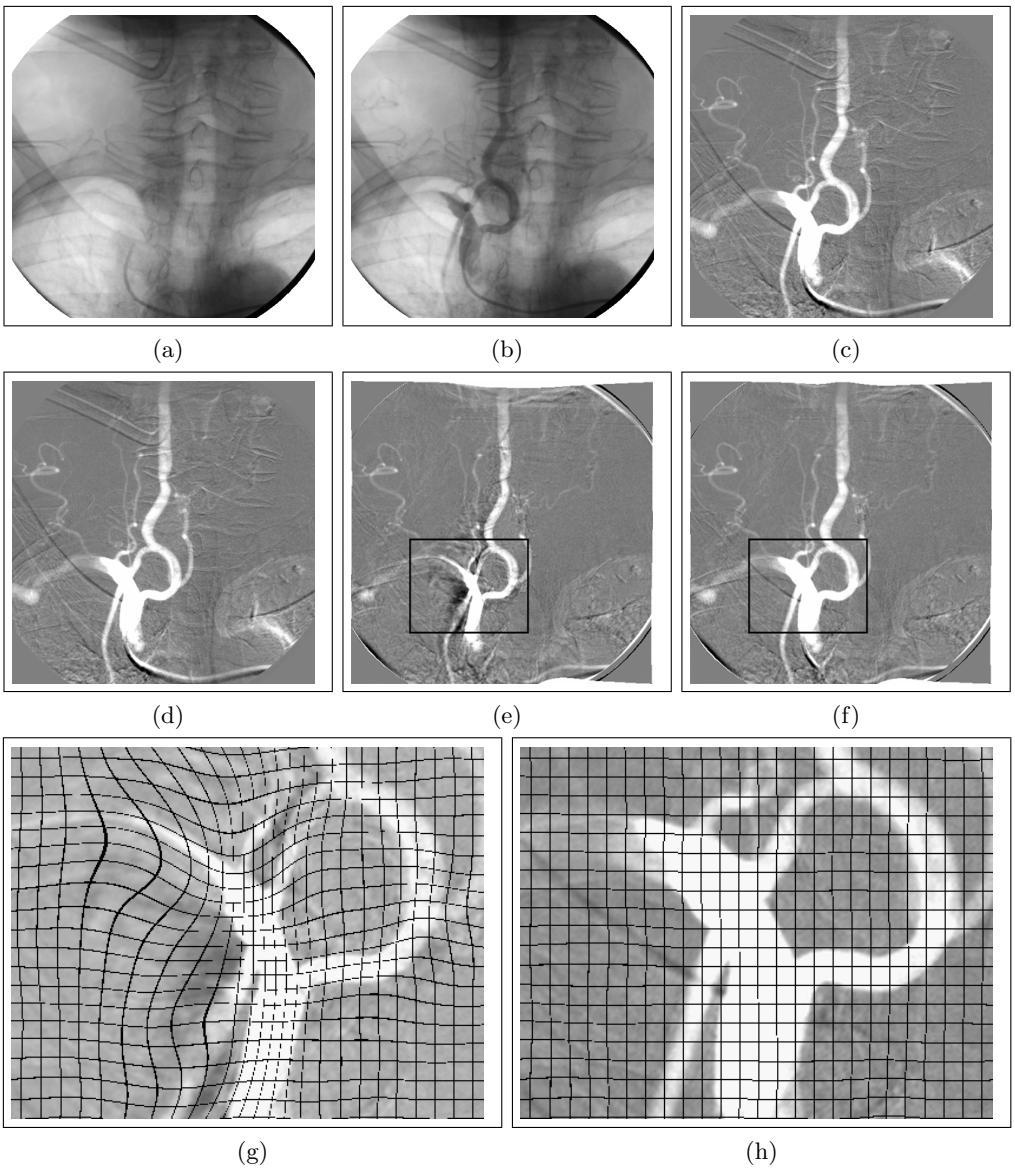

Figure 4: Comparison of registration with and without $\mathcal{S}^{\text{rigid}}[\boldsymbol{u}]$ for 2D DSA images. The vessels are to be kept rigid, while motion artifacts are to be reduced by the registration. (a) DSA base image; the fixed image, (b) DSA image after injection of the contrast bolus; the moving image. (c) - (f) are difference images with the fixed image, (c) with the moving image, (d) with the result of rigid registration, (e) with the result of standard registration, (f) with the result of the rigidly regularised registration. The bottom row depicts parts of the resulting deformation field of the standard registration (g), and of the registration including $\mathcal{S}^{\text{rigid}}[\boldsymbol{u}]$ (h). The black box in Figure (e) and (f) denotes the part of the deformation field that is depicted.

Figure 5: The six locations where the vessel diameter is measured.

	none	rigid	without $\mathcal{S}^{\text{rigid}}[\boldsymbol{u}]$	with $\mathcal{S}^{\text{rigid}}[\boldsymbol{u}]$
MSD	189.45	167.67	100.60	96.83
location 1	19.0	19.0	20.0	19.0
location 2	23.0	23.0	18.0	24.0
location 3	19.0	19.0	15.0	19.0
location 4	8.0	8.0	8.0	8.0
location 5	15.0	15.0	11.0	16.0
location 6	38.0	38.0	22.0	37.0

Table 2: The mean square difference of the background of the difference image is given, together with the vessel diameters (in pixels) at the locations defined in Figure 5.

by the mean square difference (MSD) between the result of registration and the fixed image:

$$\text{MSD} = \frac{1}{|\mathcal{B}|} \sum_{\boldsymbol{x} \in \mathcal{B}} \Big(F(\boldsymbol{x}) - M(\boldsymbol{x} + \boldsymbol{u}(\boldsymbol{x})) \Big)^2, \tag{9}$$

where the background $\mathcal{B}$ is defined as all pixels within the cone beam, but outside the vessel segmentation. From Table 2 we can see that the MSD of the background decreases for nonrigid registration, indicating removal of motion artifacts.

The compression of the vasculature is evaluated by manually measuring the vessel diameter at several locations. The locations are shown in Figure 5. From Table 2 we can see that the diameter of the vessels decreases for standard nonrigid registration, and it is preserved when the rigidity constraint is applied.

4. CONCLUSIONS AND FUTURE WORK

We introduced a novel rigidity constraint, which penalises nonrigid deformations at locations where it is required. The effectiveness of the proposed rigidity constraint is demonstrated on 2D synthetic examples, on 2D CT follow-up slices of the thorax, and on 2D DSA images. The penalty term $\mathcal{S}^{\text{rigid}}[\boldsymbol{u}]$ is shown to be a feasible way to force rigidity of certain objects while performing nonrigid registration.

When using 3 resolutions and 300 iterations in each resolution, the computation time of both registration algorithms are in the order of a couple of minutes on a standard PC (3GHz CPU and 1GB internal memory). When including the rigidity constraint in the registration the computation time increases with 40 - 50 % for the 2D images we have tested it on.

Future work includes the extension of the software to 3D and further evaluation on a set of 2D and 3D images.

ACKNOWLEDGMENTS

This research was funded by the Netherlands Organisation for Scientific Research (NWO). This work also benefited from the use of the Insight Segmentation and Registration Toolkit (ITK), an open source software developed as an initiative of the U.S. National Library of Medicine and available at `www.itk.org`.

REFERENCES

1. D. Rueckert, L. I. Sonoda, C. Hayes, D. L. G. Hill, M. O. Leach, and D. J. Hawkes, "Nonrigid registration using free-form deformations: Application to breast MR images," *IEEE Transactions on Medical Imaging* **18**(8), pp. 712 – 721, 1999.
2. D. Mattes, D. Haynor, H. Vesselle, T. Lewellen, and W. Eubank, "PET-CT image registration in the chest using free-form deformations," *IEEE Transactions on Medical Imaging* **22**(1), pp. 120 – 128, 2003.
3. T. Rohlfing, C. R. Maurer Jr., D. A. Bluemke, and M. A. Jacobs, "Volume-preserving nonrigid registration of MR breast images using free-form deformation with an incompressibility constraint," *IEEE Transactions on Medical Imaging* **22**(6), pp. 730 – 741, 2003.
4. C. Tanner, J. A. Schnabel, D. Chung, M. J. Clarkson, D. Rueckert, D. L. G. Hill, and D. J. Hawkes, "Volume and shape preservation of enhancing lesions when applying nonrigid registration to a time series of contrast enhancing MR breast images," in *Medical Image Computing and Computer-Assisted Intervention (MICCAI)*, *Lecture Notes in Computer Science* **1935**, pp. 327 – 337, 2000.
5. T. Rohlfing and C. R. Maurer Jr., "Intensity-based nonrigid registration using adaptive multilevel free-form deformation with an incompressibility constraint," in *Medical Image Computing and Computer-Assisted Intervention (MICCAI)*, *Lecture Notes in Computer Science* **2208**, pp. 111 – 119, 2001.
6. G. E. Christensen and H. J. Johnson, "Consistent image registration," *IEEE Transactions on Medical Imaging* **20**(7), pp. 568 – 582, 2001.
7. B. Fischer and J. Modersitzki, "A unified approach to fast image registration and a new curvature based registration technique," *Linear Algebra and its Applications* **380**, pp. 107 – 124, 2004.
8. J. A. Little, D. L. G. Hill, and D. J. Hawkes, "Deformations incorporating rigid structures," *Computer Vision and Image Understanding* **66**(2), pp. 223 – 232, 1997.
9. P. Thévenaz and M. Unser, "Optimization of mutual information for multiresolution image registration," *IEEE Transactions on Image Processing* **9**(12), pp. 2083 – 2099, 2000.
10. S. Klein, M. Staring, and J. P. W. Pluim, "Comparison of gradient approximation techniques for optimisation of mutual information in nonrigid registration," in *SPIE Medical Imaging: Image Processing*, *Proceedings of SPIE* **5747**, pp. 192 – 203, 2005.
11. M. Unser, "Splines: A perfect fit for signal and image processing," *IEEE Signal Processing Magazine* **16**(6), pp. 22 – 38, 1999.